Loss of the tyrosine phosphatase PTPRD leads to aberrant STAT3 activation and promotes gliomagenesis

Berenice Ortiz[a,b], Armida W. M. Fabius[b], Wei H. Wu[b], Alicia Pedraza[b], Cameron W. Brennan[c], Nikolaus Schultz[d], Kenneth L. Pitter[e], Jacqueline F. Bromberg[f], Jason T. Huse[g], Eric C. Holland[h,i], and Timothy A. Chan[b,j,1]

[c]Department of Neurosurgery, [d]Department of Computational Biology, [f]Department of Medicine, [g]Department of Pathology, and [j]Department of Radiation Oncology, [b]Human Oncology and Pathogenesis Program, [a]Gerstner Sloan-Kettering Graduate School of Biomedical Sciences, Memorial Sloan-Kettering Cancer Center, New York, NY 10065; [e]Tri-Institutional MD/PhD Program, Weill Cornell Medical College, New York, NY 10065; [h]Division of Human Biology and Solid Tumor Translational Research, Fred Hutchinson Cancer Research Center, Seattle, WA 98109; and [i]Department of Neurosurgery and Alvord Brain Tumor Center, University of Washington, Seattle, WA 98195

Edited by Bert Vogelstein, The Johns Hopkins University, Baltimore, MD, and approved April 21, 2014 (received for review February 3, 2014)

***PTPRD*, which encodes the protein tyrosine phosphatase receptor-δ, is one of the most frequently inactivated genes across human cancers, including glioblastoma multiforme (GBM). *PTPRD* undergoes both deletion and mutation in cancers, with copy number loss comprising the primary mode of inactivation in GBM. However, it is unknown whether loss of *PTPRD* promotes tumorigenesis in vivo, and the mechanistic basis of PTPRD function in tumors is unclear. Here, using genomic analysis and a glioma mouse model, we demonstrate that loss of *Ptprd* accelerates tumor formation and define the oncogenic context in which *Ptprd* loss acts. Specifically, we show that in human GBMs, heterozygous loss of *PTPRD* is the predominant type of lesion and that loss of *PTPRD* and the *CDKN2A/p16*^{INK4A} tumor suppressor frequently co-occur. Accordingly, heterozygous loss of *Ptprd* cooperates with *p16* deletion to drive gliomagenesis in mice. Moreover, loss of the Ptprd phosphatase resulted in phospho-Stat3 accumulation and constitutive activation of Stat3-driven genetic programs. Surprisingly, the consequences of *Ptprd* loss are maximal in the heterozygous state, demonstrating a tight dependence on gene dosage. *Ptprd* loss did not increase cell proliferation but rather altered pathways governing the macrophage response. In total, we reveal that PTPRD is a bona fide tumor suppressor, pinpoint *PTPRD* loss as a cause of aberrant STAT3 activation in gliomas, and establish *PTPRD* loss, in the setting of *CDKN2A/p16*^{INK4A} deletion, as a driver of glioma progression.**

Glioblastoma multiforme (GBM) is a devastating disease. It is the most common and aggressive type of glioma and outcomes remain poor despite current treatments (1). To increase our understanding of the genetic basis of this malignancy, several mutational survey studies examining GBM have been completed and provide a detailed view of the molecular changes underlying this cancer (2–4). Because GBM is a highly heterogeneous tumor, a challenge remains to determine which molecular alterations drive tumorigenesis and to understand the underlying mechanisms of action. Recent work by our group and others have identified inactivation of protein tyrosine phosphatase receptor-δ (*PTPRD*) as a frequent alteration in GBM and other tumors, and showed that *PTPRD* copy number loss correlates with poor prognosis (5–10). Despite the high prevalence of *PTPRD* inactivation in human tumors, it is not known whether loss of *PTPRD* can promote tumorigenesis. Furthermore, the mechanisms of action and the oncogenic context in which PTPRD acts remain obscure.

PTPRD belongs to a family of protein-tyrosine phosphatases that collectively have been implicated in functions, including the regulation of receptor tyrosine kinases, growth, cell migration, and angiogenesis (11). Previously, we demonstrated that phosphorylated STAT3 (p-STAT3) is a substrate of PTPRD and that cancer-specific mutations in *PTPRD* abrogate the ability of the phosphatase to dephosphorylate STAT3 (5). Interestingly, accumulation of phosphorylated STAT3 and STAT3 hyperactivation are frequent events in solid tumors like GBM, yet the genetic basis of aberrant STAT3 activation is poorly understood. p-STAT3 has been implicated in a number of tumor-promoting processes, including blocking differentiation, maintaining the stem cell pool, promoting growth and angiogenesis, and regulating the immune response and tumor microenvironment (12–14). In this study, we show that allelic loss of *Ptprd* results in p-Stat3 accumulation and Stat3 hyperactivation, elucidating one genetic root cause for aberrant STAT3 activation in GBM.

Chromosome 9p, a region frequently lost in gliomas, contains the genes encoding *PTPRD* and the cyclin dependent kinase inhibitor 2A (*CDKN2A*). The *CDKN2A* locus produces the p16^{INK4A} and p14/p19^{ARF} tumor suppressors by alternate splicing (15). We and others have shown that selective pressure exists for inactivation of both *PTPRD* and *CDKN2A*, on chromosome 9p, in many types of cancer (5, 6, 10, 16). Both genes are frequently deleted or mutated. In this study, we develop a murine tumor model in which we inactivate both genes to model the genetic events that occur on 9p. We demonstrate that *Ptprd* loss cooperates with *Cdkn2a* deletion to promote tumorigenesis.

We define the cooperative effects of PTPRD and CDKN2A by using *Ptprd* knockout and *Cdkn2a/p16*^{Ink4a} knockout mice in conjunction with the replication-competent avian sarcoma-leukosis virus long terminal repeat with splice acceptor retrovirus (RCAS) PDGFB/*Nestin*-tvA glioma mouse model. In this well-established RCAS model, the PDGFB oncogene drives glioma formation. PDGFB is specifically introduced into Nestin-expressing glial progenitor cells via infection of the avian RCAS virus into mice that express the avian tvA receptor under the *Nestin* promoter

Significance

Protein tyrosine phosphatase receptor-δ (*PTPRD*) is a frequently inactivated tumor-suppressor gene. We demonstrate that *Ptprd* inactivation in the context of *Cdkn2a/p16*^{Ink4a} deletion is sufficient to promote tumorigenesis in vivo. Our mouse model closely recapitulates the genetic events on chromosome 9p that occur in cancer. We demonstrate that PTPRD is a haploinsufficient tumor suppressor and provide a rationale for the high frequency of heterozygous loss of *PTPRD* in human glioblastoma. Finally, this study establishes loss of *PTPRD*, a STAT3 phosphatase, as a cause of STAT3 hyperactivation in gliomas.

Author contributions: B.O., A.W.M.F., J.F.B., and T.A.C. designed research; B.O., A.W.M.F., W.H.W., A.P., N.S., and K.L.P. performed research; B.O., C.W.B., N.S., K.L.P., and E.C.H. contributed new reagents/analytic tools; B.O., A.W.M.F., C.W.B., N.S., and J.T.H. analyzed data; B.O., A.W.M.F., and T.A.C. wrote the paper; and J.T.H. conducted pathology tumor grade analysis.

The authors declare no conflict of interest.

This article is a PNAS Direct Submission.

Data deposition: The data reported in this paper have been deposited in the Gene Expression Omnibus (GEO) database, www.ncbi.nlm.nih.gov/geo (accession no. GSE55061).

[1]To whom correspondence should be addressed. E-mail: chant@mskcc.org.

This article contains supporting information online at www.pnas.org/lookup/suppl/doi:10.1073/pnas.1401952111/-/DCSupplemental.

GENETICS

(17–19). Intracranial gliomas generated by the RCAS PDGFB/*Nestin* tvA mouse model reflect the histology of human GBM (20). Furthermore, as opposed to traditional genetically engineered mouse models, genes can be introduced into adult somatic cells of mice with excellent temporal specificity (19). Here, we show that *Ptprd* is a haploinsufficient tumor suppressor that cooperates with deletion of *Cdkn2a*/$p16^{Ink4a}$ to promote glioma progression.

Results

Genetic Patterns of *PTPRD* Loss in Human GBM. Previously, we showed that the *CDKN2A* and *PTPRD* genes are both commonly inactivated regions on chromosome 9p with distinct focal deletions at each locus, indicating that each gene is a minimal commonly deleted region. Furthermore, both genes are subject to somatic mutation and hypermethylation, and are hypothesized to be cancer driver genes. We set out to define GBM alterations that co-occur most frequently with *PTPRD* loss. Fig. 1*A* illustrates the co-occurrence of select GBM alterations with *PTPRD* loss in GBM tumors from the The Cancer Genome Atlas dataset. *CDKN2A*/*CDKN2B* deletions co-occurred most frequently with *PTPRD* loss ($P < 0.05$) (Table S1). Importantly, the vast majority of tumors that lose *PTPRD* also lose *CDKN2A*. Interestingly, 87% of the tumors with *PTPRD* deletion only lost one copy (Fig. 1*B*).

Heterozygous Loss of *Ptprd* Cooperates with *Cdkn2a/p16^{Ink4a}* Deletion to Promote Gliomagenesis. To investigate the functional significance of concurrent *Ptprd* and *Cdkn2a* loss in tumorigenesis, we used the RCAS PDGFB/*Nestin*-tvA proneural glioma mouse model. As shown in Table S2, *PTPRD* loss occurs in tumors of all GBM subgroups, including the proneural transcriptional subclass, which is characterized by PDGF activity. We crossed *Ptprd* knockout mice with $p16^{Ink4a}$ knockout; *Nestin*-tvA (*N*-tvA) mice to generate $Ptprd^{+/+}p16^{-/-}$;*N*-tvA, $Ptprd^{+/-}p16^{-/-}$;*N*-tvA, and $Ptprd^{-/-}p16^{-/-}$;*N*-tvA mice. We then injected neonatal mice intracranially with DF-1 chicken cells expressing RCAS PDGFB virus. Because our glioma tumor model is dependent on Nestin expression, we first measured Nestin expression in uninjected neonatal mice by flow cytometry analysis and confirmed that Nestin is unaltered by *Ptprd* loss (Fig. S1). Symptom-free survival was measured by observing the mice for the onset of brain tumor symptoms, including hydrocephalus, seizure, or general malaise. Interestingly, $Ptprd^{+/-}p16^{-/-}$ mice showed significantly worse survival than $Ptprd^{+/+}p16^{-/-}$ mice ($P < 0.05$) (Fig. 2*A*). In contrast, $Ptprd^{-/-}p16^{-/-}$ mice only showed a trend toward worse survival (Fig. 2*A*), consistent with a somewhat weaker phenotype. To our knowledge, these are the first data to show that *Ptprd* loss promotes tumorigenesis and that heterozygous loss is sufficient to do so in the context of $p16^{Ink4a}$ deletion.

To confirm that *Ptprd* was heterozygous in the tumors, tumor cells were sorted from RCAS PDGF GFP-injected *Ptprd* heterozygous mice and PCR genotyped for *Ptprd*. As illustrated in Fig. 2*B*, tumors from *Ptprd* heterozygous mice retain one intact wild-type allele. H&E-stained tumors were graded according to criteria set by the World Health Organization (21). Interestingly, as shown in Fig. 2*C*, there were no significant differences in tumor grade between the genotypes, suggesting that Ptprd may affect other processes that regulate glioma initiation or progression.

Intriguingly, when mice with *Ptprd* loss but wild-type $p16^{Ink4a}$ were injected with RCAS PDGFB virus, the mice had significantly better symptom-free survival than $Ptprd^{+/+}p16^{+/+}$ mice (Fig. S2*A*). Although survival and incidence were affected by *Ptprd* loss, there were no significant differences in tumor grade among the genotypes (Fig. S2*B*). In an effort to determine whether increased cell death could explain why $Ptprd^{+/-}p16^{+/+}$ and $Ptprd^{-/-}p16^{+/+}$ mice had better survival, we stained the tumors for cell death by TUNEL staining. As shown in Fig. S2*C*, no significant differences in TUNEL staining were observed between the genotypes. Nevertheless, our data suggest that loss of $p16^{Ink4a}$ is required in the context of *Ptprd* loss for enhanced tumorigenesis. These results may also help explain why *PTPRD* is almost never lost alone but nearly always with *CDKN2A*.

Heterozygous Loss of *Ptprd* Results in p-Stat3 Accumulation and Activation of Stat3-Dependent Transcription. Using in vitro methods, we previously identified p-STAT3 as a candidate substrate of PTPRD (5). It is well-known that p-STAT3 functions as a transcription factor for genes involved in the tumorigenic process (12, 14). We performed p-Stat3 immunohistochemistry (IHC) on glioma tumors from $Ptprd^{+/+}p16^{-/-}$, $Ptprd^{+/-}p16^{-/-}$, and $Ptprd^{-/-}p16^{-/-}$ mice. Interestingly, p-Stat3 was significantly elevated in only the $Ptprd^{+/-}p16^{-/-}$ mice (Fig. 3 *A* and *B*). Total Stat3 levels remained at similar levels between the genotypes, suggesting that the main effect is on the phosphorylation status of Stat3 (Fig. 3*A*). To determine if the increased p-Stat3 was inducing transcription of its gene targets, we measured gene-expression changes in the $Ptprd^{+/+}p16^{-/-}$, $Ptprd^{+/-}p16^{-/-}$, and $Ptprd^{-/-}p16^{-/-}$ tumors. Glioma tumor cells were purified by flow sorting and expression microarray analysis was performed. Consistent with the IHC results, microarray analysis of the tumor cells showed increased expression of known p-Stat3 gene targets in only the $Ptprd^{+/-}p16^{-/-}$ tumors (Fig. 3C and Table S3). To determine whether the changes in the phosphorylation status of STAT3 are also present in human GBM, we determined the relative levels of p-STAT3 in human tumors with varying *PTPRD* status. p-STAT3/STAT3 protein expression was measured by Western blot analysis in $PTPRD^{+/+}CDKN2A^{-/-}$ and $PTPRD^{+/-}CDKN2A^{-/-}$ tumors. p-STAT3 was significantly increased in $PTPRD^{+/-}CDKN2A^{-/-}$ tumors (Fig. 3*D*). Because of the low frequency of homozygous deletion of *PTPRD* in human GBM, $PTPRD^{-/-}CDKN2A^{-/-}$ tumors were not available for quantification. These data show that heterozygous loss of *PTPRD* and deletion of *CDKN2A*/$p16^{INK4A}$ is sufficient for accumulation of nuclear p-STAT3 and the induction of p-STAT3 gene targets.

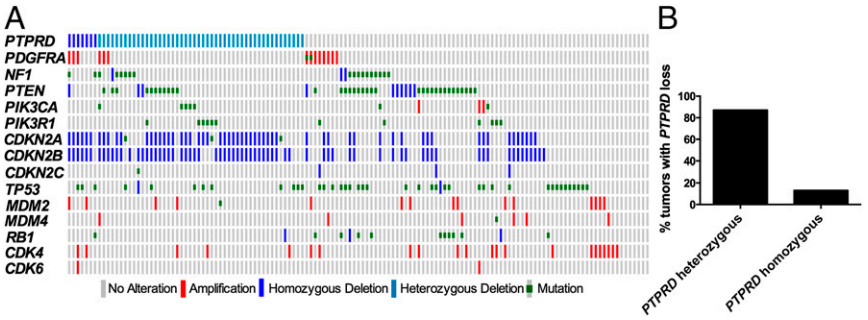

Fig. 1. Genetic context of *PTPRD* loss in human GBM. (*A*) *PTPRD* loss co-occurs most frequently with deletion of *CDKN2A* and *CDKN2B*. OncoPrint of *PTPRD* with common GBM alterations (The Cancer Genome Atlas dataset, cBio Cancer Genomics Portal). Type of alterations are as labeled in the color legend. (*B*) Frequency of heterozygous or homozygous loss of *PTPRD* in tumors with *PTPRD* loss.

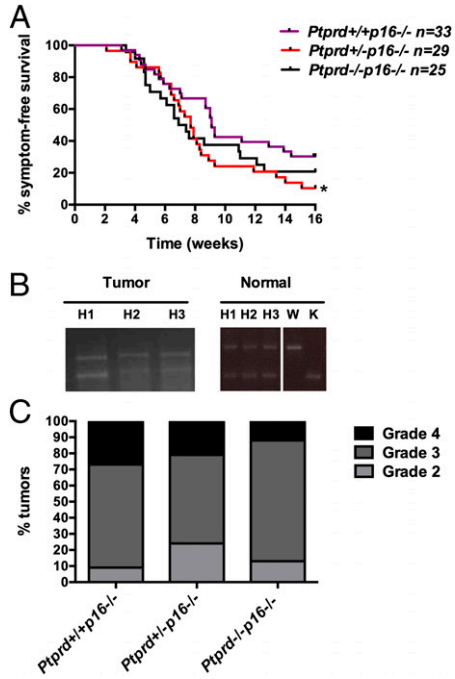

Fig. 2. *Ptprd* loss cooperates with *Cdkn2a/p16*^{Ink4a} deletion to promote gliomagenesis. (*A*) Kaplan–Meier survival curve of mice injected intracranially with DF-1–expressing RCAS-PDGFB at postnatal days 1–3 and followed for 16 wk. *Ptprd*$^{+/+}$*p16*$^{-/-}$ (n = 33), *Ptprd*$^{+/-}$*p16*$^{-/-}$ (n = 29), and *Ptprd*$^{-/-}$*p16*$^{-/-}$ (n = 25) mice. **Ptprd*$^{+/-}$p16$^{-/-}$ vs. *Ptprd*$^{+/+}$p16$^{-/-}$ $P < 0.05$. (*B*) PCR genotyping of tumor and normal tissue for *Ptprd* demonstrate that tumors from *Ptprd*$^{+/-}$*p16*$^{-/-}$ mice retain an intact wild-type allele. Mice were injected with RCAS PDGFB-GFP, and DNA was extracted from DAPI^{-} GFP^{+} tumor cells. Matched ear samples were taken for normal tissue DNA extraction. *Ptprd*$^{+/-}$*p16*$^{-/-}$ (H), *Ptprd*$^{+/+}$*p16*$^{-/-}$ (W), *Ptprd*$^{-/-}$*p16*$^{-/-}$ (K). (*C*) Tumor grade of gliomas from RCAS mice. H&E-stained tumors were graded according to World Health Organization standards. Genotypes of the mice are as indicated.

***Ptprd* Loss Does Not Increase the Rate of Cell Proliferation or Expand the Glial Progenitor Pool.** We first evaluated whether *Ptprd* loss affected tumor size by generating a separate cohort of *Ptprd*$^{+/+}$*p16*$^{-/-}$, *Ptprd*$^{+/-}$*p16*$^{-/-}$, and *Ptprd*$^{-/-}$*p16*$^{-/-}$ mice that were stereotactically injected with DF-1 cells expressing RCAS PDGFB virus. Stereotactic injection allows the precise measurement of tumor size. At a defined time-point before the development of symptoms, we performed MRI to measure the volume of the gliomas in all genotypes. As expected, there was substantial heterogeneity across the gliomas because of differences in tumor penetrance, as frequently occurs for this cancer type. Interestingly, *Ptprd*$^{+/-}$*p16*$^{-/-}$ mice showed a strong trend toward having the greatest tumor volume, suggesting that *Ptprd* loss is associated with larger tumor size (Fig. 4 *A* and *B*).

We next determined whether loss of *Ptprd* was increasing the rate of cell proliferation, decreasing the rate of cell death, expanding the glial progenitor pool, or promoting angiogenesis. We used flow cytometry to measure the frequency of K_i67 in GFP^{+} tumor cells (RCAS-infected cells coexpress GFP). Surprisingly, no significant differences in K_i67 were found among the genotypes (Fig. 4*C*). We also measured cell death in the tumors by TUNEL IHC. As shown in Fig. 4*D*, there were no significant differences in the levels of TUNEL staining between the genotypes. To determine the differentiation status of the tumor cells, we performed IHC to stain tumors from *Ptprd*$^{+/+}$*p16*$^{-/-}$, *Ptprd*$^{+/-}$*p16*$^{-/-}$, and *Ptprd*$^{-/-}$*p16*$^{-/-}$ mice for oligodendrocytes (Olig2), astrocytes (Gfap), and glial progenitors (Nestin). No differences were found in the quantity or intensity of staining between mice of the different genotypes (Fig. S3*A*). To examine the glial progenitor pool, we also performed side population analysis of the tumors, as previously described (22). No differences in the amount of side population cells for each genotype were evident, suggesting that *Ptprd* loss does not expand the glial progenitor pool (Fig. S3 *B* and *C*). Finally, we performed IHC to examine endothelial cells (CD34) and to determine if *Ptprd* loss affects angiogenesis. No differences in the quantity or intensity of staining were evident (Fig. S3*D*). Taken together, these data demonstrate that the effects of *Ptprd* loss and resultant Stat3 activation do not promote tumorigenesis by altering cellular proliferation, cellular death, cellular differentiation, or vascular density.

***Ptprd* Loss Activates Pathways That Regulate the Immune Response and Tumor Microenvironment.** To evaluate the nature of the gene-expression changes induced by *Ptprd* loss in our glioma model, we performed gene-expression analysis of sorted GFP^{+} tumor cells from *Ptprd*$^{+/+}$*p16*$^{-/-}$, *Ptprd*$^{+/-}$*p16*$^{-/-}$, and *Ptprd*$^{-/-}$*p16*$^{-/-}$ mice. Principal component analysis and hierarchical clustering demonstrated that the transcriptome of *Ptprd*$^{+/-}$*p16*$^{-/-}$ tumors is significantly different from those of *Ptprd*$^{+/+}$p16$^{-/-}$ and *Ptprd*$^{-/-}$*p16*$^{-/-}$ tumors (Fig. S4 *A* and *B*). To determine if other tyrosine phosphatases were compensating for loss of *Ptprd* in the tumors at the transcriptional level, we analyzed gene expression of other tyrosine phosphatases. As shown in Fig. S4*C* and Table S4 no significant differences between the genotypes were observed.

Pathway analysis of the differentially expressed genes in the *Ptprd*$^{+/-}$*p16*$^{-/-}$ vs. *Ptprd*$^{+/+}$*p16*$^{-/-}$ tumor cells showed statistically significant enrichment in pathways governing the immune response and macrophage behavior (Fig. 5*A* and Table S5). A fascinating pattern emerged when we reviewed the expression levels of all known cytokines and chemokines. Tumor cells from *Ptprd* heterozygotes, but not wild-type or homozygotes, had a concerted and significant increase in the expression of chemokines CCL2, CCL6, CCL12, and CXCL14 (Fig. 5*B*). All four chemokines promote M2 protumor polarization of macrophages (23–26). Thus, our gene-expression analysis suggests that loss of *Ptprd* in the tumor cells might lead to the activation of genetic programs that affect the immune response, and in particular macrophages.

There is substantial evidence that the immune response (including macrophage activity) influences tumor pathogenicity (27–29). Pyonteck et al. showed that protumor macrophages in RCAS PDGF gliomas increase tumor aggressiveness (30). To determine whether macrophages were present in the tumors from our mice, we stained *Ptprd*$^{+/+}$*p16*$^{-/-}$, *Ptprd*$^{+/-}$*p16*$^{-/-}$, and *Ptprd*$^{-/-}$*p16*$^{-/-}$ tumors with the Iba1 macrophage marker. Although the quantity of Iba1^{+} cells was similar for all tumors, we noted that tumors from *Ptprd*$^{+/-}$*p16*$^{-/-}$ tended to have amoeboid macrophage morphology, which is associated with a protumorigenic phenotype (25, 31, 32) (Fig. 5*C*); this was concentrated in the larger tumors. p-Stat3 is a marker of M2 protumor polarized macrophages (28, 33). To determine whether macrophages in our tumors might be M2 polarized, we performed immunofluorescence for Iba1 and p-Stat3 and quantified the number of cells that were Iba1^{+} and p-Stat3^{+}. Tumors in the *Ptprd*$^{+/-}$*p16*$^{-/-}$ group had greater numbers of double-positive Iba1 and p-Stat3 cells than the other genotypes (Fig. 5 *D* and *E*). These were again concentrated in the larger tumors. We also determined whether glial cells in tumors with heterozygous loss of *Ptprd* also expressed p-Stat3. We performed immunofluorescence for Gfap and p-Stat3. Tumors in the *Ptprd*$^{+/-}$*p16*$^{-/-}$ group had cells that were both p-Stat3^{+} and Gfap^{+}, as well as cells that were p-Stat3^{+} and Gfap^{-} (Fig. S5). Taken together, our data suggest that heterozygous loss of *Ptprd* activates genetic programs regulating immune response and promotes the expression of chemokines that influence immune cell behavior and macrophage biology.

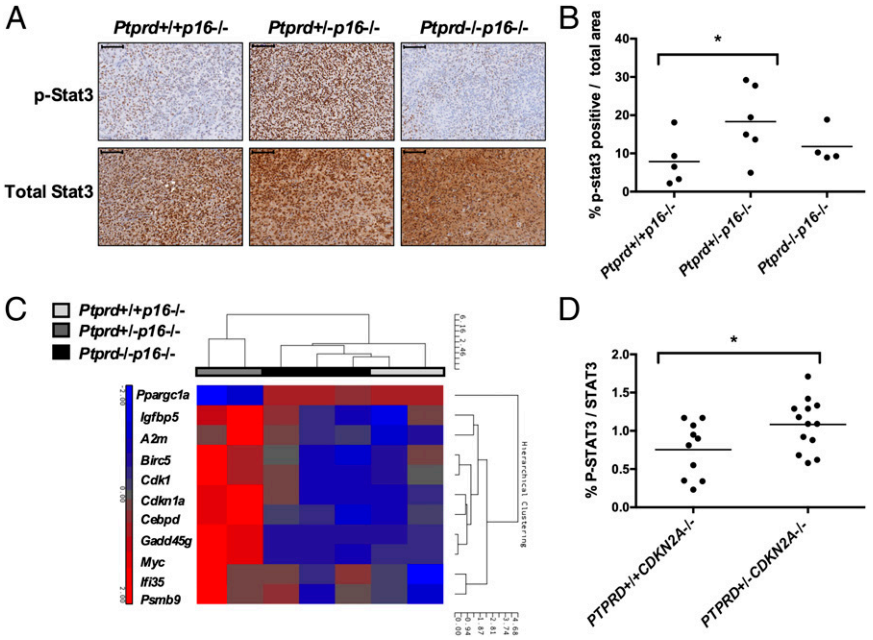

Fig. 3. Heterozygous loss of *Ptprd* results in increased p-Stat3 and activation of Stat3 gene expression. (*A*) Representative images of immunohistochemistry for p-Stat3 and Stat3 in RCAS-PDGFB induced tumors from $Ptprd^{+/+}p16^{-/-}$ ($n = 5$), $Ptprd^{+/-}p16^{-/-}$ ($n = 6$), and $Ptprd^{-/-}p16^{-/-}$ ($n = 4$) mice. (Scale bars, 100 μm.) (*B*) Quantification of IHC results showing that levels of p-Stat3 are significantly higher in tumors of $Ptprd^{+/-}p16^{-/-}$ mice, $*Ptprd^{+/-}p16^{-/-}$ vs. $Ptprd^{+/+}p16^{-/-}$ $P = 0.05$. (*C*) Expression of p-Stat3 gene targets are elevated in $Ptprd^{+/-}p16^{-/-}$ mice. Heat-map of the most variant p-Stat3 target genes across all genotypes from GFP^{+} sorted tumor cells of RCAS-PDGFB-GFP injected mice. Results from microarray analysis. $P < 0.05$, Fold-change > 1.8, $Ptprd^{+/+}p16^{-/-}$ ($n = 2$), $Ptprd^{+/-}p16^{-/-}$ ($n = 2$), $Ptprd^{-/-}p16^{-/-}$ ($n = 3$). (*D*) Amount of p-STAT3 protein is increased in $PTPRD^{+/-}CDKN2A^{-/-}$ human GBM tumors. Quantification of Western blot analysis for p-STAT3 and STAT3 in GBM tumors. $*P < 0.05$.

Discussion

Our results describe a number of important, novel observations. To begin with, and to our knowledge, we provide the first evidence that *Ptprd* loss, in the setting of *Cdkn2a*/$p16^{Ink4a}$ deletion and PDGFB overexpression, can promote better growth of tumors in vivo. Second, we show that *Ptprd* heterozygous loss and *Cdkn2a*/$p16^{Ink4a}$ deletion is sufficient to promote tumorigenesis, which supports a rationale for the patterns of *PTPRD* loss observed in human GBM and other tumor types. Third, our data indicate that heterozygous loss of *Ptprd*, a phosphatase targeting Stat3, causes p-Stat3 accumulation and Stat3 activation in murine tumors, a finding that was validated in human GBMs. This finding places PTPRD in the growing list of tumor suppressors that display haploinsufficiency. Finally, we show that *Ptprd* loss promotes tumor growth via a noncanonical means, perhaps by altering the immune response.

Our findings show that heterozygous loss of *PTPRD* most commonly co-occurs with homozygous deletion of *CDKN2A*/$p16^{INK4A}$ in human GBM. We generated an in vivo glioma model of *Ptprd* and *Cdkn2a*/$p16^{Ink4a}$ deletion to study the contribution of each chromosome 9p gene to gliomagenesis. Importantly, mice with *Ptprd* loss and $p16^{Ink4a}$ deletion had worse survival than mice with $p16^{Ink4a}$ deletion alone. These observations demonstrate that loss of these two 9p tumor suppressors cooperate and influence tumorigenesis in a context-dependent fashion. Interestingly, *Ptprd* loss in the context of wild-type $p16^{Ink4a}$ demonstrated better survival. Staining for TUNEL, a marker for cell death, showed that increased cell death does not explain the better survival. Nevertheless, it is clear that in the context of our mouse model, $p16^{Ink4a}$

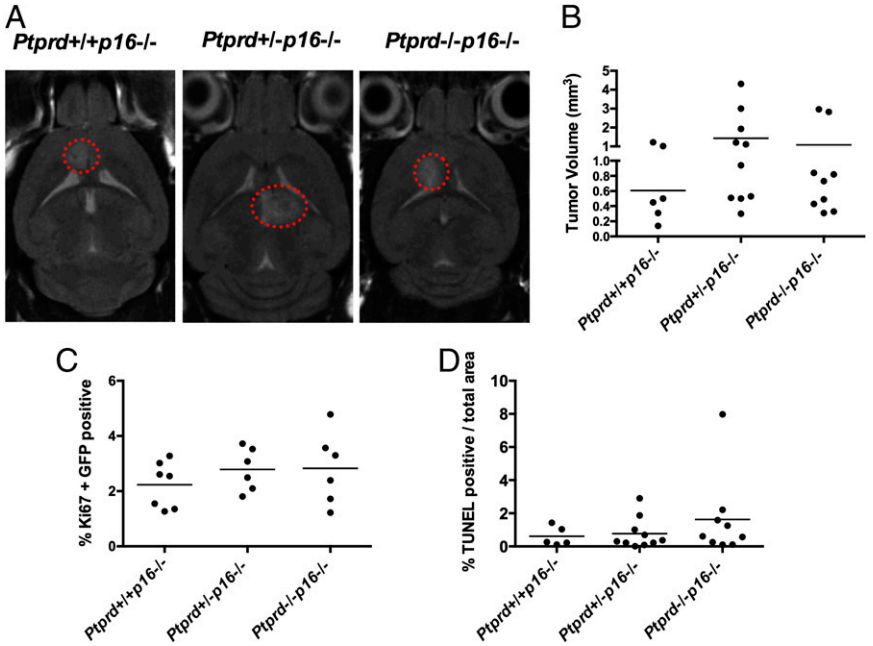

Fig. 4. *Ptprd* loss does not promote increased cell proliferation. (*A*) Representative MRI images of $Ptprd^{+/+}p16^{-/-}$ ($n = 6$), $Ptprd^{+/-}p16^{-/-}$ ($n = 10$), and $Ptprd^{-/-}p16^{-/-}$ ($n = 9$) tumors from mice that were stereotactically injected with DF-1 cells expressing RCAS-PDGFB. The presence of a tumor was confirmed by histology. (*B*) $Ptprd^{+/-}p16^{-/-}$ mice show a trend toward having larger tumors (defined as >0.7 mm^3). Quantification of tumor size from MRI images. (*C*) *Ptprd* loss does not increase levels of cell proliferation in gliomas. No significant differences in the levels of K_i67 were observed within the tumor cells of $Ptprd^{+/+}p16^{-/-}$ ($n = 7$), $Ptprd^{+/-}p16^{-/-}$ ($n = 6$), and $Ptprd^{-/-}p16^{-/-}$ ($n = 6$) mice. K_i67 flow cytometry analysis was performed on GFP^{+} tumor cells from RCAS PDGFB-GFP tumors. (*D*) *Ptprd* loss does not alter the levels of cell death in gliomas. Quantification of immunohistochemistry results show that no significant differences in the levels of TUNEL staining were observed in the tumors of stereotactically injected $Ptprd^{+/+}p16^{-/-}$ ($n = 5$), $Ptprd^{+/-}p16^{-/-}$ ($n = 10$), and $Ptprd^{-/-}p16^{-/-}$ ($n = 9$) mice.

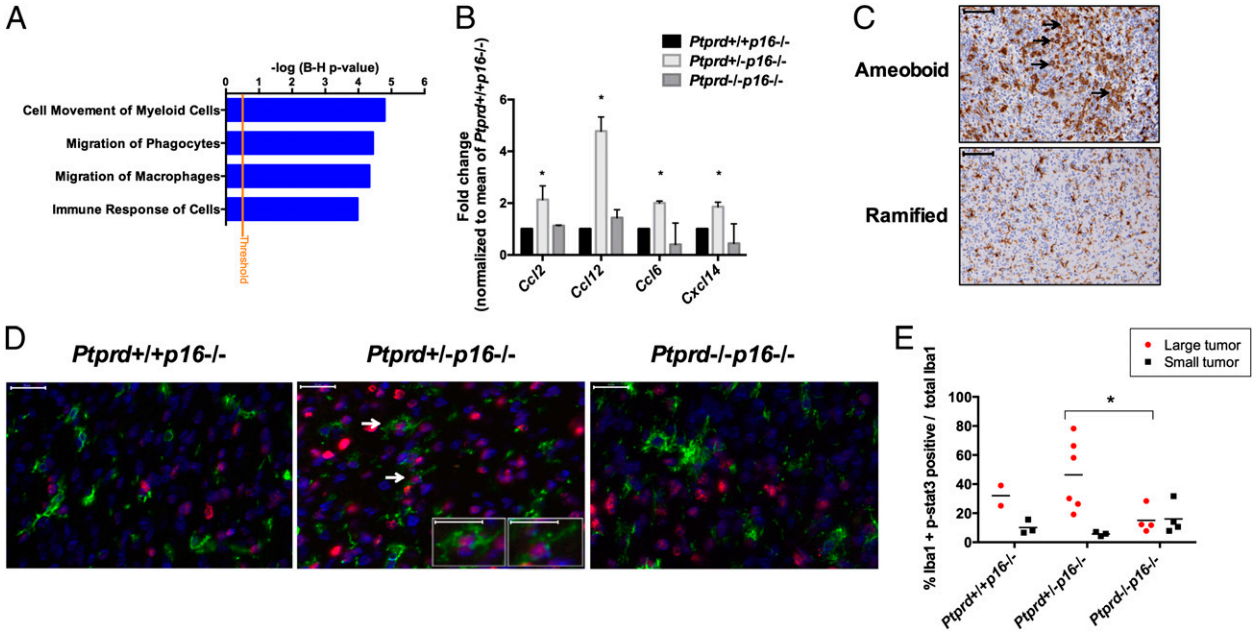

Fig. 5. Heterozygous loss of *Ptprd* activates immune programs and influences the macrophage response. (*A*) Immune response gene-expression pathways are activated in $Ptprd^{+/-}p16^{-/-}$ tumors. Gene-expression microarray analysis was performed on GFP^+ tumor cells from $Ptprd^{+/+}p16^{-/-}$ ($n = 2$), $Ptprd^{+/-}p16^{-/-}$ ($n = 2$), and $Ptprd^{-/-}p16^{-/-}$ ($n = 3$) mice. A selection of the top activated pathways enriched in the differentially expressed genes of $Ptprd^{+/-}p16^{-/-}$ vs. $Ptprd^{+/+}p16^{-/-}$ tumors are shown, false-discovery rate $P < 0.05$. (*B*) Expression of chemokines that promote M2 polarization of macrophages is increased in $Ptprd^{+/-}p16^{-/-}$ tumors. Fold-change of chemokine expression normalized to mean of $Ptprd^{+/+}p16^{-/-}$ expression from microarray analysis. Error bars = 1 SD. $Ptprd^{+/+}p16^{-/-}$ ($n = 2$), $Ptprd^{+/-}p16^{-/-}$ ($n = 2$), and $Ptprd^{-/-}p16^{-/-}$ ($n = 3$). *$Ptprd^{+/-}p16^{-/-}$ vs. $Ptprd^{+/+}p16^{-/-}$ $P < 0.05$. (*C*) Examples of tumors stained with the Iba1 macrophage marker. Arrows indicate locations of amoeboid macrophages. Amoeboid morphology is enriched in large tumors and ramified macrophages mainly occur in smaller tumors (large tumors defined as >0.7 mm^3 tumor volume). Examples from $Ptprd^{+/-}p16^{-/-}$ mice (amoeboid) and $Ptprd^{+/+}p16^{-/-}$ mice (ramified). (Scale bars, 100 μm.) (*D*) Representative images of Iba1 and p-Stat3 immunofluorescence on tumors from indicated genotypes. Green, Iba1; blue, DAPI; red, p-Stat3. (Large image scale bars, 20 μm.) White arrows indicate cells with nuclear p-Stat3 and cytoplasmic Iba1 and are enlarged (*Insets*) (Scale bars, 10 μm.) (*E*) $Ptprd^{+/-}p16^{-/-}$ large tumors have greater p-Stat3 expression in $Iba1^+$ macrophages. Metamorph quantification of $Iba1^+$ and $p\text{-}Stat3^+$ cells, *$Ptprd^{+/-}p16^{-/-}$ *vs.* $Ptprd^{-/-}p16^{-/-}$ (large tumors) $P < 0.05$.

loss is required for enhancing tumorigenesis. These results are consistent with the high level of concordance between genetic events targeting the two genes in human GBM.

Perhaps most interesting were our observations pertaining to *Ptprd* gene dosage: poorer survival, altered gene expression, increased p-Stat3, and increased production of chemokines all occurred to a greater extent when *Ptprd* was heterozygous. This finding suggests that heterozygous loss of *PTPRD* is sufficient to promote tumorigenesis in the setting of *CDKN2A* deletion. However, our findings were somewhat unexpected, because a classic haploinsufficient tumor suppressor typically produces at least equivalent (or more severe) functional impact in the homozygous setting. In contrast, complete abrogation of Ptprd resulted in a paradoxical decrease in intensity of observable phenotypes, which suggests that PTPRD dosage is critical. It is possible that complete abrogation of PTPRD ultimately leads to activation of a negative-feedback loop in STAT3 signaling, which is what down-regulates the pathway. Indeed, negative feedback is well established in STAT3 signaling and can exist at many levels. In our mouse models, we may be observing the consequences of negative-feedback inhibition when tonic Stat3 hyperactivation exceeds a threshold, as previously observed (34–36). Furthermore, STAT3 signaling pathways are subject to significant cross-talk. It is possible that when both alleles of *PTPRD* are deleted, other partially redundant phosphatases are induced and bring p-STAT3 levels down to below that found in *PTPRD* heterozygous tumors (37). However, we measured the gene-expression levels of other tyrosine phosphatases in our microarray to determine if these changes were occurring at the transcriptional level. No significant differences were observed between the genotypes, suggesting that compensation by other tyrosine phosphatases may be occurring at the posttranslational level. Additional work will need to be done to elucidate the intricacies of these signaling pathways. Nevertheless, our data provide one potential explanation of why the vast majority of *PTPRD* genetic alterations (both somatic mutation and copy number loss) in human cancers are heterozygous.

Another intriguing and novel aspect of our study was that *PTPRD* loss appears to act not primarily by promoting cell division or blocking differentiation, but by altering the tumor microenvironment. Our gene-expression analysis of the tumor cells demonstrated that activation of genetic programs governing immune response and macrophage response were at play. More specifically, $Ptprd^{+/-}p16^{-/-}$ tumors had activated genes involved in up-regulation of several chemokines, all of which promote M2 polarization (23–26). Macrophages can enhance tumor cell survival by promoting tumor growth, invasion, or immunosuppression (27–29, 38–40). In addition, recent work by Pyonteck et al. showed that RCAS PDGFB gliomas have tumor-associated macrophages, and that inhibiting their polarization state can significantly improve survival (30). Several studies demonstrate that p-Stat3 within macrophages polarizes them to a M2 tumor-promoting state (28, 33). We show that $Ptprd^{+/-}p16^{-/-}$ tumors had higher levels of p-Stat3 in macrophages, demonstrating that *Ptprd* loss can affect p-Stat3 accumulation in the macrophages and may alter the macrophage state.

In summary, we show that *Ptprd* loss with $Cdkn2a/p16^{Ink4a}$ deletion can promote gliomagenesis. These findings have substantial implications for our understanding of a commonly mutated

tumor suppressor gene as well as for our comprehension of the novel mechanisms that can be used to promote gliomagenesis.

Materials and Methods

See *SI Materials and Methods* for full methods.

Mouse Model. *P16$^{Ink4a-/-}$;Nestin*-tvA mice were kindly provided by Eric Holland (Memorial Sloan-Kettering Cancer Center, New York, NY) (41, 42). *Ptprd$^{+/-}$* mice were generously provided by Michael Tremblay (McGill University, Montreal, QC, Canada) (43). All mice experiments were performed under Memorial Sloan-Kettering Cancer Center (MSKCC) Institutional Animal Care and Use Committee approval.

Sorted GFP^{+} tumor cells from mice injected with RCAS PDGF-GFP were extracted using the DNeasy Blood and Tissue kit (Qiagen). PCR was performed with the following *Ptprd* genotyping primers: 5′-GGTGAAGTGTGACCAGTATTGGCC3′, 5′CTGGAATTGTCTCACTTTCCTC-3′, and 5′-GACTGCCTTGGGAAAAGCGCCTCC-3′. Standard PCR procedures were performed with the following reaction buffer: 1 M $(NH_4)2SO_4$, 2 M Tris, pH 8.8, 1 M $MgCl_2$, and 14.4 M B-mercaptoethanol.

Cell Culture and RCAS Virus. RCAS retrovirus was propagated in chicken DF-1 cells (ATCC, CRL-12203). The transfection of DF-1 cells with RCAS vectors were performed with Lipofectamine 2000 (Life Technologies). Intracranial injections into neonatal mice were used to introduce DF-1 cells expressing RCAS virus as described previously (44). RCAS-PDGF-HA and RCAS-PDGF-GFP viral expression plasmids were a gift from Eric Holland (Memorial Sloan-Kettering Cancer Center, New York, NY) and have been previously described (20, 45). Mice were monitored daily and killed upon demonstration of brain tumor symptoms (hydrocephalus, hunched, or seizure) or at 16 wk of age.

Stereotactic injections of DF-1 cells propagating RCAS-PDGF-HA virus was performed in adult mice 7–10 wk old. Injections into the subventricular zone were performed as described previously (18). The following coordinates for the subventricular zone were used: Bregma 0 mm, lateral right of midline −0.5 mm, and depth of 1.5 mm from the dural surface. Mice were monitored daily and killed upon demonstration of brain tumor symptoms or at 23-wk postinjection.

ACKNOWLEDGMENTS. We thank Daniel Ciznadija and Sevin Turcan for helpful advice; Afsar Barlas, Dmitry Yarilin, Sho Fujisawa, and Ke Xu of the Molecular Cytology Core Facility at MSKCC for immunohistochemistry and immunofluorescence staining and analysis; and the MSKCC Comparative Pathology Core Facility, the MSKCC Research Animal Resource Center, the MSKCC Small Imaging Core Facility, the MSKCC Genomics Core Facility, and the MSKCC Flow Cytometry Sorting Core Facility for excellent technical assistance. This project was supported by Grants F31CA171566 (to B.O.) and R01CA154767 (to T.A.C.) from the National Institutes of Health. Partial support was provided by the Molecular Cytology Core Facility Grant P30CA008748.

1. Stupp R, et al.; European Organisation for Research and Treatment of Cancer Brain Tumor and Radiotherapy Groups; National Cancer Institute of Canada Clinical Trials Group (2005) Radiotherapy plus concomitant and adjuvant temozolomide for glioblastoma. *N Engl J Med* 352(10):987–996.
2. Cancer Genome Atlas Research Network (2008) Comprehensive genomic characterization defines human glioblastoma genes and core pathways. *Nature* 455(7216):1061–1068.
3. Verhaak RG, et al.; Cancer Genome Atlas Research Network (2010) Integrated genomic analysis identifies clinically relevant subtypes of glioblastoma characterized by abnormalities in PDGFRA, IDH1, EGFR, and NF1. *Cancer Cell* 17(1):98–110.
4. Parsons DW, et al. (2008) An integrated genomic analysis of human glioblastoma multiforme. *Science* 321(5897):1807–1812.
5. Veeriah S, et al. (2009) The tyrosine phosphatase PTPRD is a tumor suppressor that is frequently inactivated and mutated in glioblastoma and other human cancers. *Proc Natl Acad Sci USA* 106(23):9435–9440.
6. Solomon DA, et al. (2008) Mutational inactivation of PTPRD in glioblastoma multiforme and malignant melanoma. *Cancer Res* 68(24):10300–10306.
7. Boeva V, et al. (2013) Breakpoint features of genomic rearrangements in neuroblastoma with unbalanced translocations and chromothripsis. *PLoS ONE* 8(8):e72182.
8. Du Y, et al. (2013) Polymorphism in protein tyrosine phosphatase receptor delta is associated with the risk of clear cell renal cell carcinoma. *Gene* 512(1):64–69.
9. Meehan M, et al. (2012) Protein tyrosine phosphatase receptor delta acts as a neuroblastoma tumor suppressor by destabilizing the aurora kinase A oncogene. *Mol Cancer* 11:6.
10. Cancer Genome Atlas Network (2012) Comprehensive molecular portraits of human breast tumours. *Nature* 490(7418):61–70.
11. Ostman A, Hellberg C, Böhmer FD (2006) Protein-tyrosine phosphatases and cancer. *Nat Rev Cancer* 6(4):307–320.
12. Brantley EC, Benveniste EN (2008) Signal transducer and activator of transcription-3: A molecular hub for signaling pathways in gliomas. *Mol Cancer Res* 6(5):675–684.
13. Carro MS, et al. (2010) The transcriptional network for mesenchymal transformation of brain tumours. *Nature* 463(7279):318–325.
14. Bournazou E, Bromberg J (2013) Targeting the tumor microenvironment: JAK-STAT3 signaling. *JAK-STAT* 2(2):e23828.
15. Sherr CJ (2001) The INK4a/ARF network in tumour suppression. *Nat Rev Mol Cell Biol* 2(10):731–737.
16. Beroukhim R, et al. (2010) The landscape of somatic copy-number alteration across human cancers. *Nature* 463(7283):899–905.
17. Uhrbom L, Holland EC (2001) Modeling gliomagenesis with somatic cell gene transfer using retroviral vectors. *J Neurooncol* 53(3):297–305.
18. Hambardzumyan D, Amankulor NM, Helmy KY, Becher OJ, Holland EC (2009) Modeling adult gliomas using RCAS/t-va technology. *Transl Oncol* 2(2):89–95.
19. Orsulic S (2002) An RCAS-TVA-based approach to designer mouse models. *Mamm Genome* 13(10):543–547.
20. Dai C, et al. (2001) PDGF autocrine stimulation dedifferentiates cultured astrocytes and induces oligodendrogliomas and oligoastrocytomas from neural progenitors and astrocytes in vivo. *Genes Dev* 15(15):1913–1925.
21. Louis DN, et al. (2007) The 2007 WHO classification of tumours of the central nervous system. *Acta Neuropathol* 114(2):97–109.
22. Bleau AM, et al. (2009) PTEN/PI3K/Akt pathway regulates the side population phenotype and ABCG2 activity in glioma tumor stem-like cells. *Cell Stem Cell* 4(3):226–235.
23. Roca H, et al. (2009) CCL2 and interleukin-6 promote survival of human CD11b+ peripheral blood mononuclear cells and induce M2-type macrophage polarization. *J Biol Chem* 284(49):34342–34354.
24. Murray PJ, Wynn TA (2011) Protective and pathogenic functions of macrophage subsets. *Nat Rev Immunol* 11(11):723–737.
25. Gabrusiewicz K, et al. (2011) Characteristics of the alternative phenotype of microglia/macrophages and its modulation in experimental gliomas. *PLoS ONE* 6(8):e23902.
26. Movahedi K, et al. (2010) Different tumor microenvironments contain functionally distinct subsets of macrophages derived from Ly6C(high) monocytes. *Cancer Res* 70(14):5728–5739.
27. da Fonseca AC, Badie B (2013) Microglia and macrophages in malignant gliomas: Recent discoveries and implications for promising therapies. *Clin Dev Immunol* 2013:264124.
28. Li W, Graeber MB (2012) The molecular profile of microglia under the influence of glioma. *Neuro-oncol* 14(8):958–978.
29. Hao NB, et al. (2012) Macrophages in tumor microenvironments and the progression of tumors. *Clin Dev Immunol* 2012:948098.
30. Pyonteck SM, et al. (2013) CSF-1R inhibition alters macrophage polarization and blocks glioma progression. *Nat Med* 19(10):1264–1272.
31. Sliwa M, et al. (2007) The invasion promoting effect of microglia on glioblastoma cells is inhibited by cyclosporin A. *Brain* 130(Pt 2):476–489.
32. Hanisch UK, Kettenmann H (2007) Microglia: Active sensor and versatile effector cells in the normal and pathologic brain. *Nat Neurosci* 10(11):1387–1394.
33. Zhang L, et al. (2009) Stat3 inhibition activates tumor macrophages and abrogates glioma growth in mice. *Glia* 57(13):1458–1467.
34. Ernst MB, et al. (2009) Enhanced Stat3 activation in POMC neurons provokes negative feedback inhibition of leptin and insulin signaling in obesity. *J Neurosci* 29(37):11582–11593.
35. Trilling M, et al. (2014) "Activated" STAT proteins: A paradoxical consequence of inhibited JAK-STAT signaling in cytomegalovirus-infected cells. *J Immunol* 192(1):447–458.
36. Nichane M, Ren X, Bellefroid EJ (2010) Self-regulation of Stat3 activity coordinates cell-cycle progression and neural crest specification. *EMBO J* 29(1):55–67.
37. Zhang X, et al. (2007) Identification of STAT3 as a substrate of receptor protein tyrosine phosphatase T. *Proc Natl Acad Sci USA* 104(10):4060–4064.
38. Daginakatte GC, Gutmann DH (2007) Neurofibromatosis-1 (Nf1) heterozygous brain microglia elaborate paracrine factors that promote Nf1-deficient astrocyte and glioma growth. *Hum Mol Genet* 16(9):1098–1112.
39. Simmons GW, et al. (2011) Neurofibromatosis-1 heterozygosity increases microglia in a spatially and temporally restricted pattern relevant to mouse optic glioma formation and growth. *J Neuropathol Exp Neurol* 70(1):51–62.
40. Pong WW, Higer SB, Gianino SM, Emnett RJ, Gutmann DH (2013) Reduced microglial CX3CR1 expression delays neurofibromatosis-1 glioma formation. *Ann Neurol* 73(2):303–308.
41. Uhrbom L, Hesselager G, Nistér M, Westermark B (1998) Induction of brain tumors in mice using a recombinant platelet-derived growth factor B-chain retrovirus. *Cancer Res* 58(23):5275–5279.
42. Tchougounova E, et al. (2007) Loss of Arf causes tumor progression of PDGFB-induced oligodendroglioma. *Oncogene* 26(43):6289–6296.
43. Uetani N, et al. (2000) Impaired learning with enhanced hippocampal long-term potentiation in PTPdelta-deficient mice. *EMBO J* 19(12):2775–2785.
44. Liu Y, et al. (2007) Somatic cell type specific gene transfer reveals a tumor-promoting function for p21(Waf1/Cip1). *EMBO J* 26(22):4683–4693.
45. Becher OJ, et al. (2008) Gli activity correlates with tumor grade in platelet-derived growth factor-induced gliomas. *Cancer Res* 68(7):2241–2249.